Thermal Modeling of Lundell Alternators

Sai Chun Tang, *Member, IEEE*, Thomas A. Keim, and David J. Perreault, *Member, IEEE*

***Abstract*—Thermal analysis of Lundell alternators used in automobiles is presented. An analytical thermal model for Lundell alternators is proposed, and procedures for acquiring the model parameters are elucidated. Based on the thermal model, the temperature profile of an operating Lundell alternator can be predicted analytically. The predicted alternator temperatures are found to be consistent with the experimental measurement. The presented models and measurement methods are useful for embedding switched-mode power electronics into the alternator with low manufacturing cost.**

***Index Terms*—Automobile, Lundell alternator, thermal model.**

I. Introduction

THE Lundell, or claw-pole, alternator is almost universally used for power generation in modern automobiles. Currently, a full-bridge diode rectifier is used to produce a dc output from the three-phase ac waveforms generated by the alternator. However, the continuous increase in electrical power demand in automobiles [1], [2] and the need for improved transient control and efficiency in future electrical systems [3], [4] is motivating the introduction of more sophisticated power electronics in the alternator. Such power electronics, including switched-mode rectifiers and converters, offer substantial improvements in output power, efficiency, and transient performance. For example, in [5] and [6], it is demonstrated that introduction of a switched-mode rectifier (SMR) can increase the average power capability of a conventional Lundell alternator by a factor 1.9, improve its efficiency by as much as 20%, and can virtually eliminate the large alternator load-dump transient. The introduction of power-electronic controls thus represents a means for meeting the automotive power requirements of the future while preserving the manufacturing advantages and infrastructure investment associated with Lundell machines.

Designing an alternator with integrated power electronics represents a substantial challenge. To understand this, consider that the efficiency of a conventional Lundell alternator is about 40–60%, depending on operating conditions [4], [5], [7]. The total power loss in a 2-kW alternator, for example, may be higher than 1 kW. The resulting alternator temperature could be higher than 200 °C in the underhood environment, while the junction temperature ratings of typical switching power devices is only about 175 °C. One may suggest physically separating the power electronics from the alternator and placing them in a location with lower temperature. However, this arrangement can cause electromagnetic compatibility (EMC) problems and limit alternator power due to the wiring between the alternator and rectifier. Moreover, providing separate cooling means for the electronics may greatly increase manufactured cost. A further challenge is that power-electronic controls can result in machine operating points that differ substantially from those found conventionally. This changes the dissipation and temperature profiles of the machine, which are important considerations in the design.

This paper addresses thermal modeling of Lundell alternators. The major heat sources of the alternator and means for quantifying them are identified. An analytical thermal model for automotive Lundell alternators is developed, and procedures for acquiring the model parameters are elucidated. The thermal model permits the temperature profile of an alternator to be predicted analytically. The model is validated by comparison of predicted temperature distributions to experimental results. For our purpose of incorporating electronic controls in existing machine designs, the experimental method of determining model parameters described in this paper will serve us quite well. In other instances, the model parameters may be calculated, for example, by the finite-element method. No matter how the parameters are obtained, the reasonable agreement between the temperatures predicted by our model and observed on experiment show that the thermal model presented here can be useful for the design of future alternators.

II. Structure of Lundell Alternator

A typical Lundell alternator used in automobiles is shown in Fig. 1. It can be mainly divided into two parts–the alternator machine and the rectifier. The alternator machine consists of a rotor and a stator. The field winding is wound around the rotor. The pulley mounted at the front end of the rotor shaft is driven by a belt. The cross-sectional view of the alternator machine is illustrated in Fig. 2. There are three stator windings accommodated inside the slots of the stator core and the angular displacement between the windings is 120° electrical phase. The stator windings are isolated from the stator core by slot insulators, as shown in Fig. 3. The stator core is tightly surrounded by the alternator case. The winding-to-insulator and the insulator-to-core contact areas are much smaller than the core-to-case contact area. Therefore, the contact thermal resistance between the stator windings and the stator core is much higher than that between the stator core and the alternator case. Apart from the factor of contact resistance, the relatively high thermal resistance of the slot insulator, compared with the core material, causes the winding-to-core thermal resistance to be much higher than the core-to-case thermal resistance.

Two fans, mounted on the rotor shaft and located at the two ends of the rotor, provide forced convection cooling for both the alternator machine and the rectifier. When the rotor rotates, the

Manuscript received March 17, 2003; revised September 16, 2003. Paper no. TEC-00061-2003.

The authors are with the Laboratory for Electromagnetic and Electronic Systems, Massachusetts Institute of Technology, Cambridge, MA 02139 USA (e-mail: djperrea@mit.edu).

Digital Object Identifier 10.1109/TEC.2004.837289

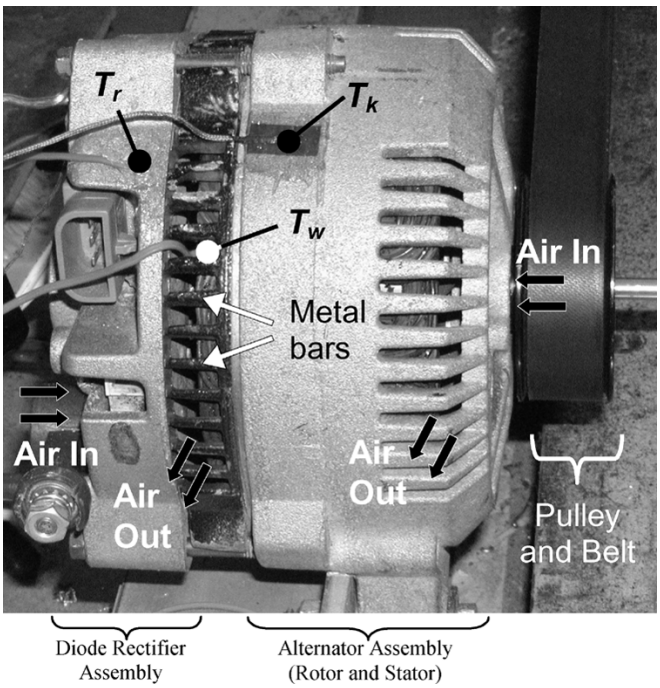

Fig. 1. Typical Lundell alternator.

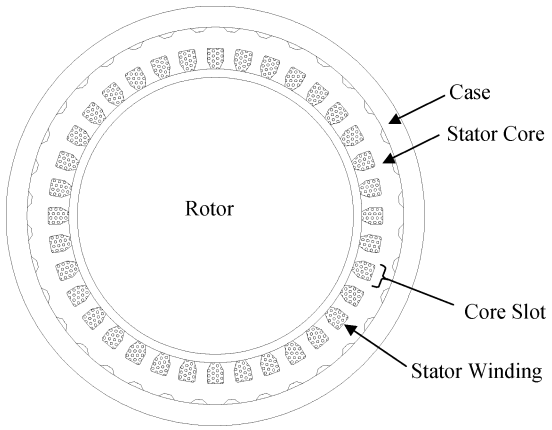

Fig. 2. Cross-sectional view of the alternator machine.

fans force the ambient air to flow into the alternator through the end windows and to flow out through the side windows, as illustrated in Fig. 1. This air flow takes away the heat energy generated in the alternator machine and the rectifier. As the alternator speed increases, the rate of air flow increases and, therefore, the cooling effect increases.

As shown in Fig. 1, the diode rectifier assembly is separated from the alternator machine with metal bars. The small cross-sectional area of the metal bar structure increases the thermal resistance between the diode plates and the high-temperature stator case. Moreover, air flowing through the windows between bars cools down the bars. This metal bar structure is, therefore, an effective way to reduce the heat flowing into the diode plates from the stator case.

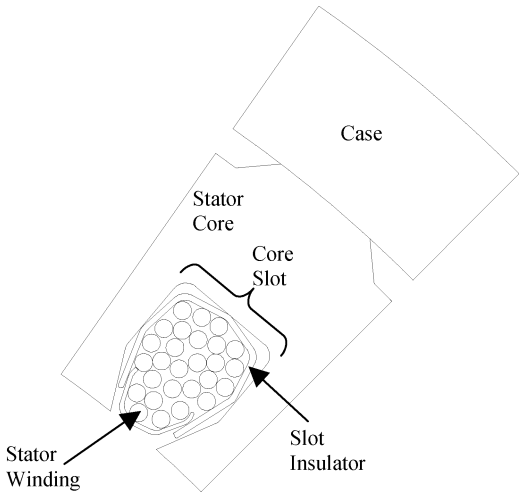

Fig. 3. Cross-sectional view of stator windings inside a core slot.

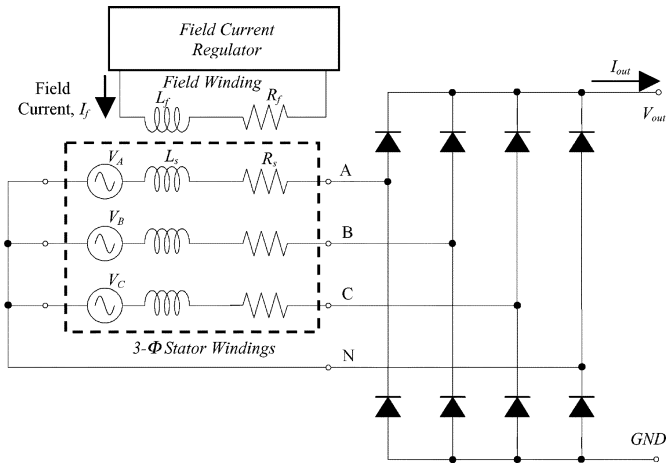

Fig. 4. Circuit schematic of a typical Lundell alternator.

III. Operating Principle and Heat Sources of the Lundell Alternator

When there is current flowing into the field winding and the rotor is turned by the belt, a rotating dc magnetic field is generated. When the rotating field cuts the three stator windings, three-phase ac voltages are induced in the three stator windings. The circuit schematic of the Lundell alternator is shown in Fig. 4. The generated three-phase ac voltage, displaced by 120° electrical phase angle, is rectified by a full-bridge diode rectifier. The fourth diode leg (connected to the neutral, N) of the full-bridge rectifier is used to increase the output power by up to 10% at high alternator speed by means of rectifying the third harmonic voltage induced in the three stator windings [4].

When a 1.7-kW alternator, for instance, is loaded with 14 Vdc, the maximum output dc current $I_{\rm out}$ is about 120 A. The maximum field current is typically less than about 4 A and the voltage across the field winding is about 14 V. The maximum power dissipation of the rotor due to conduction loss is therefore about 56 W. However, the stator core loss and the conduction loss of the stator windings range from a few hundred watts to

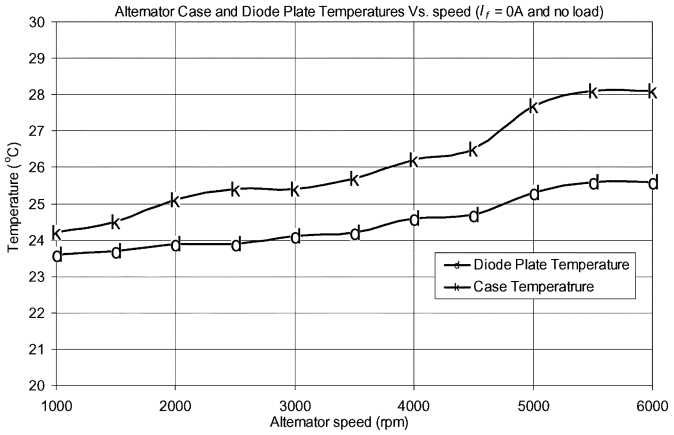

Fig. 5. Case and diode plate temperatures of the alternator under test at no-field current and no-load condition.

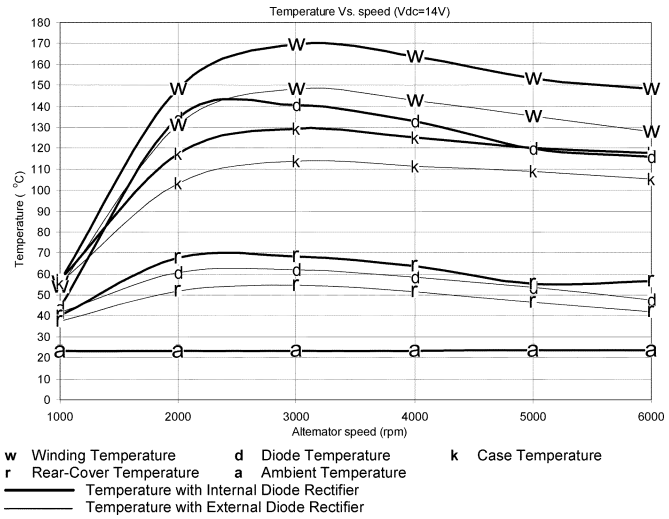

Fig. 6. Alternator temperatures versus alternator speed with 14-Vdc load condition and 3.6-A field current.

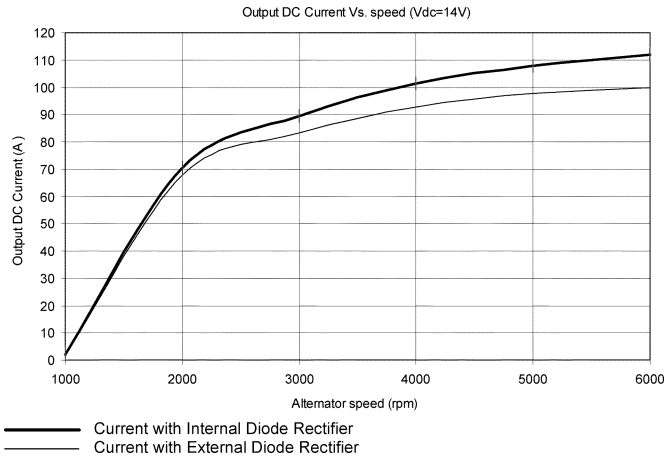

Fig. 7. Alternator output current versus alternator speed with 14 Vdc load condition and 3.6-A field current.

more than 1000 W [5], [7]. Therefore, the heat energy generated by the rotor is negligible compared with the stator losses.

Apart from the electrical losses, mechanical losses also cause temperature rise in the alternator system, especially at high speeds. These mechanical losses include the frictional losses at the contacts of the roller bearings and the slip rings, and the windage losses of the rotor and the fans. Temperature rise of a Lundell alternator due to the mechanical losses (without applying field current and load) has been measured and plotted in Fig. 5. At an ambient temperature of 22 °C, the alternator case temperature increases to about 28 °C at an alternator speed of 6000 r/min, which corresponds to the engine cruising speed. From the measured alternator temperatures, the mechanical losses cause negligible temperature rise to the alternator system compared to that including electrical losses (Fig. 6). Generally, mechanical losses of a Lundell alternator, operating at cruising speed, are very small compared to the electrical counterpart [7]. The effects of mechanical losses can, therefore, be neglected in the following thermal analysis. The main heat sources of the Lundell alternator come from the electrical losses which comprise the conduction losses of the stator windings and the diode rectifier, and the iron losses, including eddy current loss and hysteresis loss of the stator core.

IV. Temperature Profile of an Operating Lundell Alternator at 14-Vdc Load Condition

Thermocouple sensors were attached on different parts of a Lundell alternator as shown in Fig. 1 in order to measure the case temperature T_k, stator winding temperature T_w, rear-cover temperature T_r, and the diode temperature T_d. The thermocouple for measuring the diode temperature, mounted on the diode plate, is not shown in the figure because the rectifier is shielded by the rear cover. As discussed in Section III, energy dissipation from the rotor is negligible compared with that from the stator; thus, measuring the rotor temperature is not a necessity for our purposes.

The temperatures and output currents of a Lundell alternator, with both internal and external diode full-bridge rectifiers, were measured and plotted in Figs. 6 and 7, respectively. The field current is set to 3.6 A (nominal full field). The output voltage of the alternator is set to 14 Vdc by connecting an electronic load (HP 6050 A), with constant voltage (CV) mode to the alternator output terminals. Because of the high alternator output current, voltage drops across the wires connecting the electronic load to the alternator are inevitable. It is important to note that the 14 Vdc potential difference should be right across the alternator output terminals instead of across the input terminals of the electronic load. To make sure the output voltage of the alternator is set accurately, remote voltage sensing mode of the electronic load is selected and the remote sense leads are connected to the alternator output terminals.

The internal rectifier is located at the back of the alternator as shown in Fig. 1. When the external rectifier is used, no current flows through the internal rectifier and, therefore, no heat energy is generated from the internal rectifier. The use of an external rectifier, which is far away from the alternator to prevent heat conduction between the rectifier and the alternator, is to identify the effect of heat generated from the alternator machine alone on the alternator temperature distribution. Four AWG 10 wires with a length of about 2 m are used to connect the stator winding terminals to the external rectifier. The wire impedance,

including reactance and resistance, acts as an additional alternator output impedance, which limits the output current capability of the alternator. Fig. 7 illustrates the phenomenon that the output current with external diode rectifier is lower than that with an internal rectifier. It is probable that separating the rectifier from the alternator in a vehicle installation would reduce the power capability for the same reason as in the laboratory.

From Fig. 7, the alternator output currents increase drastically from 1000- to 3000-r/min alternator speed. The average output current i_o of a three-phase rectifier with a constant-voltage load can be expressed as

$$i_o \approx \frac{3}{\pi} I_{s1} \tag{1}$$

where I_{s1} is the magnitude of the fundamental component of the line currents flowing through the stator windings [8].

When the output current increases, currents flowing through the stator windings and the diode rectifier increase. Accordingly, when the alternator speed increases from 1000 to 3000 r/min, power dissipation due to conduction losses increases and, therefore, alternator temperatures increase as shown in Fig. 6. From an alternator speed of 3000 to 6000 r/min, the increase of the output current is relatively small so the increases of conduction losses of the stator windings and diodes are small. Further, as the alternator speed increases, the cooling effect due to the fans inside the alternator increases. As a result, the alternator temperatures drop when the alternator speed increases from 3000 to 6000 r/min as illustrated in Fig. 6.

Consider the case that the alternator operates with the internal rectifier; the maximum diode temperature is 140 °C. The alternator is tested at the condition of 23 °C room temperature, so the maximum temperature difference between diode and ambient $\Delta T_{da(\max)}$ is 117 °C. When the alternator operates at different ambient temperature, the alternator temperatures will change proportionally. For instance, if the diode rectifier operates at an underhood temperature of 83 °C, the maximum diode temperature could be as high as 200 °C, neglecting changes in diode loss with temperature.

As mentioned in Section II, the rear cover and the diode plates are thermally separated from the alternator case by metal bars. Fig. 1 shows the positions of the thermocouples sensing the alternator case and rear-cover temperatures. When the external rectifier is used, Fig. 6 shows that the maximum case temperature is 114 °C, but the rear-cover temperature is only 54 °C (i.e., the maximum temperature difference between the alternator case and the rear-cover is 60 °C). This shows that the metal bar structure is an effective way to resist heat flowing from the high-temperature alternator part to the diode rectifier.

V. Thermal Model for Lundell Alternators

A thermal circuit model for Lundell alternators is illustrated in Fig. 8. The analogy between the thermal circuit and electrical circuit is illustrated in Appendix A. As the power dissipation of the rotor is negligible compared with the stator losses, the heat source due to the rotor loss is ignored in the model for simplicity. The five nodes T_d, T_c, T_k, T_w, and T_a in the thermal circuit represent the temperatures of diode rectifier, stator core, alternator case, stator windings, and ambient, respectively. The power loss of the diode rectifier, the stator winding conduction loss, and the stator core losses are denoted by P_d, P_w, and P_c, respectively. R_{da}, R_{wa}, R_{ca}, and R'_{ka} represent the diode-to-ambient, stator-winding-to-ambient, stator-core-to-ambient, and case-to-ambient thermal resistance, respectively. This object-to-ambient thermal resistance describes the heat transfer from the alternator machine to the ambient by forced-air convection and heat conduction. The diode-to-case, the stator-winding-to-core, and the stator-core-to-case thermal resistance are represented by R_{dk}, R_{wc}, and R_{ck}, respectively. This object-to-object thermal resistance is mainly attributed to heat conduction between the two objects although convective effects are included.

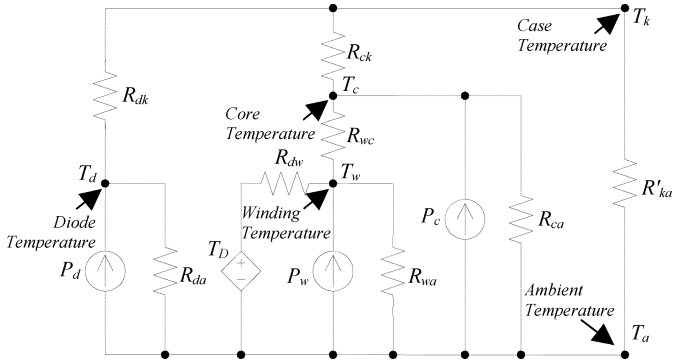

Fig. 8. Thermal model for Lundell alternators.

As shown in Fig. 1, the intake air flowing through the back windows passes through the rectifier assembly and then through part of the stator winding and ultimately flows out through the side windows. When the diode temperature is higher than the winding temperature, the winding would be heated up by the rectifier with the aid of the air flow. Similarly, when the diode temperature is lower than the winding temperature, the winding would be cooled down. In short, the winding temperature depends on the rectifier temperature. If a thermal resistor were used to represent the heat flow, it would mean that the heat flowing out from the diode and the stator windings would depend on each other's temperature. However, due to the air flow direction, heat flowing out from the diode depends on the intake air temperature but is independent of the winding temperature (if we consider the heat transfer by means of air convection only). Thus, heat transfer from the diode rectifier to the stator windings cannot be represented simply by connecting a thermal resistance between the nodes T_d and T_w.

The heat transfer due to air flow from the diode to the stator winding can be modeled by connecting a dependent temperature source T_D (analogous to the dependent voltage source in electric-circuit theory), where $T_D = T_d$ to T_w through a thermal resistance R_{dw}, as shown in Fig. 8. Because the value of the dependent temperature source T_D is equal to the diode temperature, the use of the dependent temperature source can describe how the diode temperature will affect the winding temperature. Since there is no thermal resistance directly connected between the nodes T_d and T_w, the circuit model also has the property that the diode temperature cannot be affected by the winding temperature.

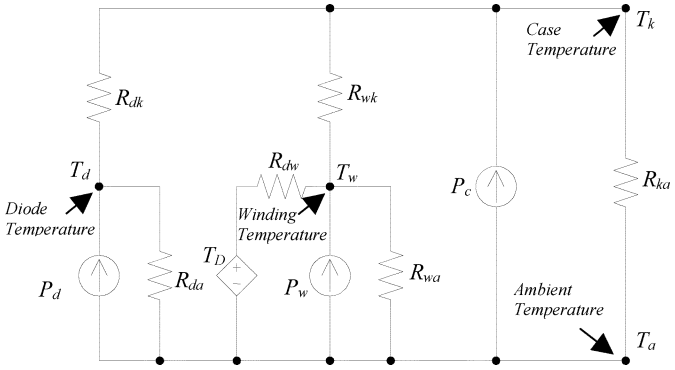

Fig. 9. Simplified thermal model for Lundell alternators.

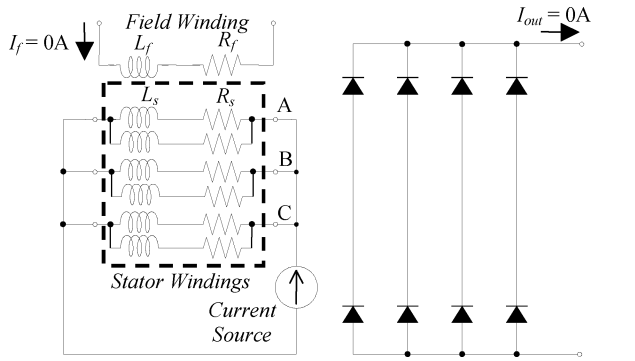

Fig. 10. Current injecting into the stator windings that generates a dc magnetic field.

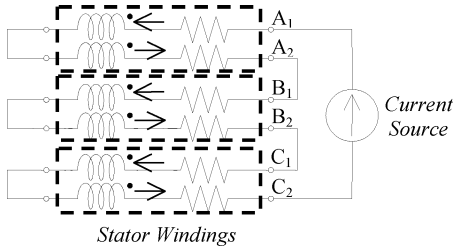

Fig. 11. Current injecting into the stator windings that generates no net magnetic field.

As explained in Section II, the stator-winding-to-core thermal resistance R_{wc} is much larger than the core-to-case thermal resistance R_{ck}. Moreover, since the values of the winding loss and the core losses of a typical Lundell alternator have the same order of magnitude, the temperature drops across R_{ck} is much smaller than that across R_{wc}. The thermal model in Fig. 8 can be simplified as shown in Fig. 9. The heat power source due to core loss P_c is assumed to flow into the alternator case directly. This neglects the drop in R_{ck} due to P_c. The thermal resistance R_{wc} and R_{ck} are combined together and expressed as winding-to-case thermal resistance R_{wk}. The thermal resistance R_{ka} in Fig. 9 represents the parallel connection of the thermal resistance R'_{ka} and R_{ca} in Fig. 8.

In the simplified thermal circuit model, the six unknown thermal resistances, at a specified alternator speed, can be found by the following procedure:

1. Set the field current to zero (to avoid generating unwanted magnetic field) by disconnecting the field winding.
2. Disconnect the rectifier so that the diode loss P_d is equal to zero.
3. Rotate the rotor at the selected speed (e.g., 1800 r/min).
4. Inject a dc current into the stator windings so that the stator windings are the heat source P_w. Maintain the power supplied to the stator windings constant. Since a dc current is applied to the stator windings, there is no stator core loss (i.e., $P_c = 0$).
5. Measure the steady state temperatures T_a, T_d, T_k, and T_w.
6. Similar to the nodal analysis in electric circuit theory, set three equations at the three nodes T_d, T_k, and T_w in the thermal circuit model.
7. Disconnect the current source from the stator windings.
8. Rotate the rotor at the selected speed.
9. Inject a dc current to the diode rectifier so that the diode rectifier becomes the heat source P_d. Maintain the power supplied to the rectifier constant.
10. Measure the steady-state temperatures T_a, T_d, T_k, and T_w.
11. Similar to the nodal analysis in electric-circuit theory, set three equations at the three nodes T_d, T_k, and T_w in the thermal circuit model.

When dc currents are injected into the diode rectifier and the stator windings, precautions must be taken to prevent the alternator from damage.

1) Apply an appropriate power level to the stator winding so that the winding temperature would not exceed its maximum value $T_{w(\max)}$ at underhood conditions. From Fig. 6, when the alternator operates at 23 °C ambient temperature, the maximum winding temperature is about 170 °C. Thus, if we assume the temperature of intake air to the alternator is 83 °C at the underhood environment, the maximum winding temperature $T_{w(\max)}$, will be about 240 °C.
2) Avoid any magnetic field induced inside the alternator. When dc current is injected into the stator windings as shown in Fig. 10, a dc magnetic field will be generated. When the rotor rotates, the iron core of the rotor will cut the dc magnetic field and, therefore, an eddy current will be induced inside the rotor core. This eddy current loss is not only an extra heat source that will affect the accuracy of the measured thermal resistance values but is also able to damage the alternator by melting the plastic layer between the rotor poles. Because each phase of the stator windings of the Lundell alternator under test is made of two copper wires connected in parallel, this eddy current problem can be resolved by connecting the stator windings and the current source as shown in Fig. 11. As current flowing through one wire is in opposite direction to

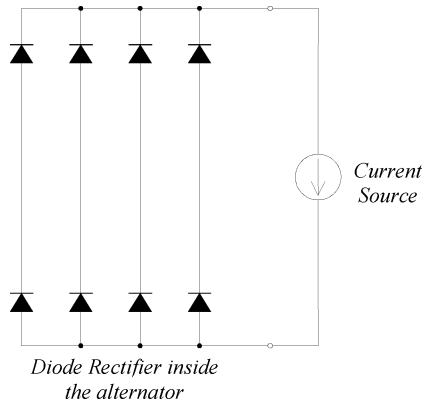

Fig. 12. Circuit schematic of injecting current into the diode rectifier.

the other wire in the same phase winding, the magnetic field generated by one wire will cancel out that generated by the other. Consequently, no net magnetic field is generated and, thus, no eddy current is induced inside the rotor core.

3) Current injected into the diode rectifier should be kept below the maximum current rating of the rectifier. A circuit schematic of injecting current into the diode rectifier is illustrated in Fig. 12.

See (2)–(7), shown at the bottom of the page.

At each rotor speed, there are six independent equations obtained from steps 6 and 11. By solving the six equations, the six thermal resistances in the thermal model for the Lundell alternators can be calculated in terms of these six measurements, as detailed in Appendix A. The solutions are (2) to (7). As mentioned in Section IV, the cooling effect increases when alternator speed increases, due to the built-in fans on the rotor. The thermal resistances of the alternator, therefore, are functions of alternator speed. In (2) to (7), the dependence on speed (ω) is explicitly indicated. However, for simplicity, the ω symbol is omitted in the equations afterward.

In the expressions of the six thermal resistances, ΔT_{xa} denotes the temperature different between object x and ambient. The subscripts with (w) denote that the temperature differences are measured when the stator windings are the heat source. The subscripts with (d) represent that the temperature differences are measured when the rectifier is the heat source.

When power of 550 W is injected into the stator winding, the temperature profile of the alternator under test at different alternator speeds is measured and shown in Fig. 13. Since the stator windings are the heat source, they are of the highest temperature. Heat transfers from the stator windings to the diode rectifier through the alternator case by heat conduction. Fig. 14 illustrates the measured alternator temperatures at different alternator speeds when 200 W of power is injected into the rectifier. The rectifier temperature is the highest since the rectifier is the heat source in this case. From the measured result, the stator winding temperature is a little higher than the alternator case temperature because heat transfers from the diode rectifier to the stator winding with the aid of the air flow from the back-end windows, through the diode rectifier, and to the stator windings as indicated in Fig. 1.

By substituting the measured alternator temperatures at different alternator speeds with $P_w = 550$ W and $P_d = 200$ W, as shown in Figs. 13 and 14, into (2) to (7), shown at the bottom of the previous page, the six thermal resistances in the simpli-

$$R_{da}(\omega) = \frac{\Delta T_{da(w)}(\omega)\cdot\lfloor\Delta T_{da(d)}(\omega) - \Delta T_{ka(d)}(\omega)\rfloor - \Delta T_{da(d)}(\omega)\cdot\lfloor\Delta T_{da(w)}(\omega) - \Delta T_{ka(w)}(\omega)\rfloor}{\left[\Delta T_{ka(w)}(\omega) - \Delta T_{da(w)}(\omega)\right]\cdot P_d} \tag{2}$$

$$R_{dk}(\omega) = \frac{\Delta T_{da(w)}(\omega)\cdot\lfloor\Delta T_{da(d)}(\omega) - \Delta T_{ka(d)}(\omega)\rfloor - \Delta T_{da(d)}(\omega)\cdot\lfloor\Delta T_{da(w)}(\omega) - \Delta T_{ka(w)}(\omega)\rfloor}{\Delta T_{da(w)}(\omega)\cdot P_d} \tag{3}$$

$$R_{ka}(\omega) = \frac{\lfloor\Delta T_{ka(d)}(\omega) - \Delta T_{wa(d)}(\omega)\rfloor\cdot\Delta T_{ka(w)}(\omega) - \lfloor\Delta T_{ka(w)}(\omega) - \Delta T_{wa(w)}(\omega)\rfloor\cdot\Delta T_{ka(d)}(\omega)}{\begin{array}{c}\left[\Delta T_{ka(d)}(\omega)-\Delta T_{wa(d)}(\omega)\right]\left[\Delta T_{da(w)}(\omega)-\Delta T_{ka(w)}(\omega)\right]\cdot\frac{1}{R_{dk}(\omega)}\\ +\left[\Delta T_{wa(w)}(\omega)-\Delta T_{ka(w)}(\omega)\right]\left[\Delta T_{da(d)}(\omega)-\Delta T_{ka(d)}(\omega)\right]\cdot\frac{1}{R_{dk}(\omega)}\end{array}} \tag{4}$$

$$R_{wk}(\omega) = \frac{\lfloor\Delta T_{ka(d)}(\omega) - \Delta T_{wa(d)}(\omega)\rfloor\cdot\Delta T_{ka(w)}(\omega) - \lfloor\Delta T_{ka(w)}(\omega) - \Delta T_{wa(w)}(\omega)\rfloor\cdot\Delta T_{ka(d)}(\omega)}{-\Delta T_{ka(d)}(\omega)\cdot\left[\Delta T_{da(w)}(\omega) - \Delta T_{ka(w)}(\omega)\right]\cdot\frac{1}{R_{dk}(\omega)} + \Delta T_{ka(w)}(\omega)\cdot\left[\Delta T_{da(d)}(\omega) - \Delta T_{ka(d)}(\omega)\right]\cdot\frac{1}{R_{dk}(\omega)}} \tag{5}$$

$$R_{dw}(\omega) = \frac{\lfloor\Delta T_{wa(w)}(\omega) - \Delta T_{da(w)}(\omega)\rfloor\cdot\Delta T_{wa(d)}(\omega) - \lfloor\Delta T_{wa(d)}(\omega) - \Delta T_{da(d)}(\omega)\rfloor\cdot\Delta T_{wa(w)}(\omega)}{\begin{array}{c}\Delta T_{wa(d)}(\omega)\cdot\left\{P_w + \left[\Delta T_{ka(w)}(\omega) - \Delta T_{wa(w)}(\omega)\right]\cdot\frac{1}{R_{wk}(\omega)}\right\}\\ -\Delta T_{wa(w)}(\omega)\cdot\left[\Delta T_{ka(d)}(\omega) - \Delta T_{wa(d)}(\omega)\right]\cdot\frac{1}{R_{wk}(\omega)}\end{array}} \tag{6}$$

$$R_{wa}(\omega) = \frac{\lfloor\Delta T_{wa(w)}(\omega) - \Delta T_{da(w)}(\omega)\rfloor\cdot\Delta T_{wa(d)}(\omega) - \lfloor\Delta T_{wa(d)}(\omega) - \Delta T_{da(d)}(\omega)\rfloor\cdot\Delta T_{wa(w)}(\omega)}{\begin{array}{c}\left[\Delta T_{da(d)}(\omega)-\Delta T_{wa(d)}(\omega)\right]\cdot\left\{P_w+\left[\Delta T_{ka(w)}(\omega)-\Delta T_{wa(w)}(\omega)\right]\cdot\frac{1}{R_{wk}(\omega)}\right\}\\ +\left[\Delta T_{wa(w)}(\omega)-\Delta T_{da(w)}(\omega)\right]\left[\Delta T_{ka(d)}(\omega)-\Delta T_{wa(d)}(\omega)\right]\frac{1}{R_{wk}(\omega)}\end{array}}. \tag{7}$$

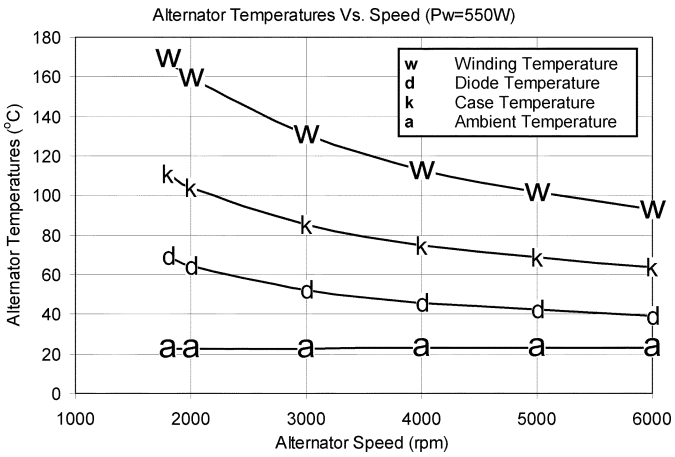

Fig. 13. Alternator temperatures versus alternator speed when power of 550 W is injected into the stator windings.

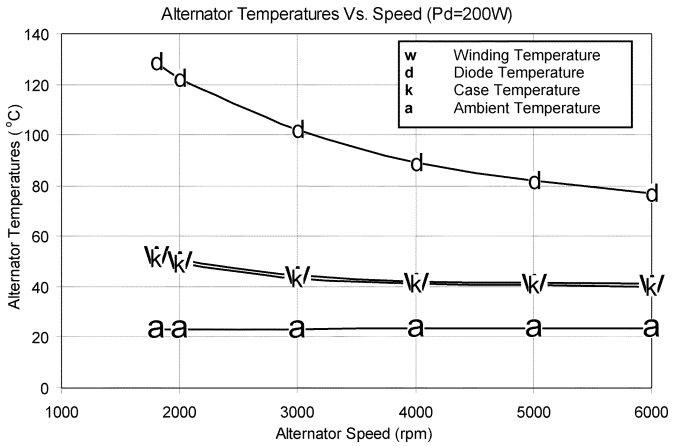

Fig. 14. Alternator temperatures versus alternator speed when power of 200 W is injected into the diode rectifier.

fied thermal circuit model can be calculated and are plotted in Fig. 15.

Because the thermal resistance R_{dw} represents the heat transfer between the diode rectifier and the stator winding by means of air flow, its value highly depends on the alternator speed. When the alternator speed increases, the rates of air flow and, thus, heat transfer from the diode rectifier to the stator windings increase. Since thermal resistance is inversely proportional to the heat-transfer rate, the thermal resistance R_{dw} decreases as the alternator speed increases. Similarly, because the object-to-ambient thermal resistance R_{xa} represents the heat transfer from an object to the ambient with the aid of air convection, the values of object-to-ambient thermal resistance R_{xa} decrease as the alternator speed increases. Because the alternator case has the largest surface area exposed to the air, the case-to-ambient thermal resistance R_{ka} is the smallest among the three object-to-ambient thermal resistance.

Due to the high thermal resistance of the metal bar structure separating the rectifier assembly from the alternator case, the diode-to-case thermal resistance R_{dk} is relatively high. Since the metal bars are cooled by the air flowing through the windows between them, the heat transfer between the diode rectifier and the alternator case is affected by the air-flow volume

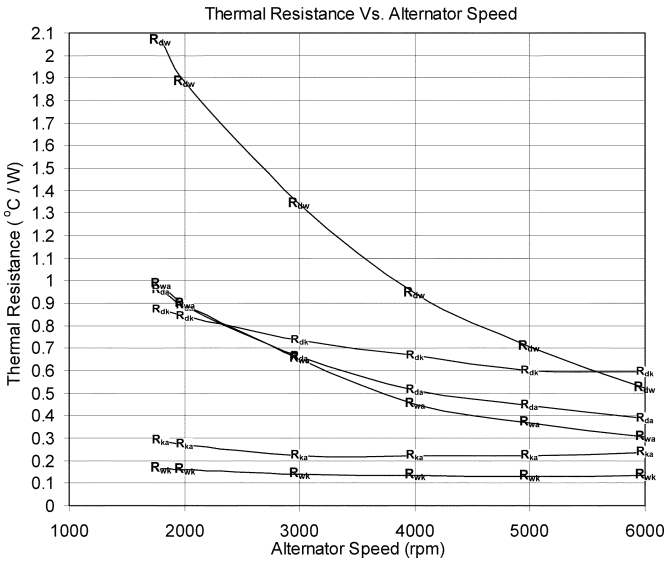

Fig. 15. Thermal resistance of the Lundell alternator under test versus alternator speed.

and temperature. Empirically, the value of R_{dk} decreases as the alternator speed increases.

The winding-to-case thermal resistance R_{wk} represents the series connection of the stator winding-to-core R_{wc} and the core-to-case R_{ck} thermal resistance. As shown in Figs. 2 and 3, the stator windings are installed inside the slots of the stator core which is tightly surrounded by the alternator case. Besides, the heat-transfer path from the stator windings to the alternator case is very short, so the winding-to-case thermal resistance R_{wk} has the smallest value among the six thermal resistances.

The simplified thermal circuit model for Lundell alternators in Fig. 9 cannot only describe the heat flows between different parts of an alternator but can also predict the temperature distribution of an operating alternator. This is valuable for the design of alternator systems incorporating switched-mode power electronics, as it enables the alternator and converter temperature distributions to be predicted under conditions that can vary substantially from these encountered with diode rectification.

Consider the thermal circuit model in Fig. 9.

At node T_d

$$\left(\frac{1}{R_{da}}+\frac{1}{R_{dk}}\right)\Delta T_{da}-\frac{1}{R_{dk}}\Delta T_{ka}=P_d. \tag{8}$$

At node T_k

$$-\frac{1}{R_{dk}}\Delta T_{da}+\left(\frac{1}{R_{dk}}+\frac{1}{R_{ka}}+\frac{1}{R_{wk}}\right)\Delta T_{ka}-\frac{1}{R_{wk}}\Delta T_{wa}=P_c. \tag{9}$$

At node T_w

$$-\frac{1}{R_{dw}}\Delta T_{da}-\frac{1}{R_{wk}}\Delta T_{ka}+\left(\frac{1}{R_{dw}}+\frac{1}{R_{wa}}+\frac{1}{R_{wk}}\right)\Delta T_{wa}=P_w. \tag{10}$$

By solving (8)–(10), the diode-to-ambient ΔT_{da}, the case-to-ambient ΔT_{ka}, and the winding-to-ambient ΔT_{wa} temperature differences can be calculated and expressed in (11)–(13), respectively. From (11)–(13), the temperature differences can be obtained when the six thermal resistance

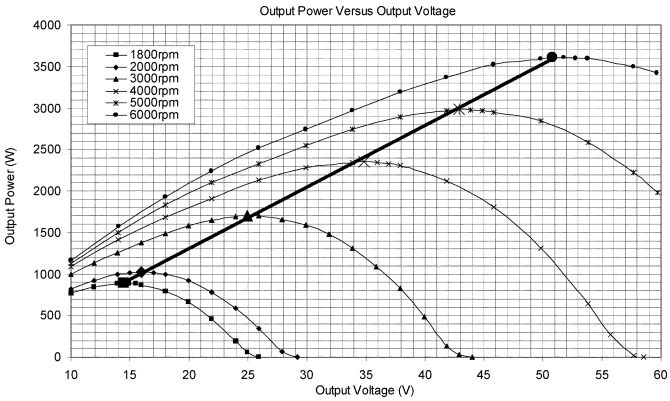

Fig. 16. Measured output power of the Lundell alternator versus alternator output voltage with different alternator speeds.

values, the stator winding loss P_w, the rectifier loss P_d, and the stator core loss P_c are known. Here, the proposed method for acquiring the thermal resistance parameters is based on temperature measurement of an actual alternator. Nevertheless, to the extent that reliable thermal FEM [9]–[11] predictions for alternator temperature rise can be made, FEM predictions for specific test conditions can be used as the inputs to generate the parameters in the proposed model.

VI. Validation of the Thermal Model

In this section, we validate the developed thermal model using the alternator of Fig. 1. In particular, we are interested in temperature profiles that occur at maximum load-matched alternator power [5], [6]. The load-matched power is the maximum power obtainable with a diode rectifier at a given speed across output voltage. It is of interest because it represents the maximum power achievable at fixed output (battery) voltage for some types of switched-mode rectifiers. We validate the model by comparing the measured alternator temperatures under load-matched conditions to those predicted by the thermal model (11) to (13), with model parameters established as described here.

The alternator output powers versus output voltage with different alternator speeds from 1800 to 6000 r/min are measured and plotted in Fig. 16. As the alternator speed increases, the output voltage at maximum output power condition increases. The relationship between the maximum output power and the corresponding output voltage, with different alternator speeds, is approximately linear as indicated by the straight line shown in Fig. 16 [5], [6]. The output voltage and current at maximum output power condition, as well as the maximum output power are plotted against the alternator speed in Fig. 17. The output voltage and maximum power increase approximately linearly from about 14.5 to 50.8 V and from about 881 to 3583 W, respectively, as the alternator speed increases from 1800 to 6000 r/min. It implies that the output voltage and maximum power increase by about 250% and 307%, respectively. However, the output current, at maximum output-power condition, increases from 61.3 to 70.6 A when the alternator speed increases from 1800 to 6000 r/min. The increase of output current is about 15%. Therefore, at the maximum output-power condition, the increase of the stator winding conduction loss is relatively small

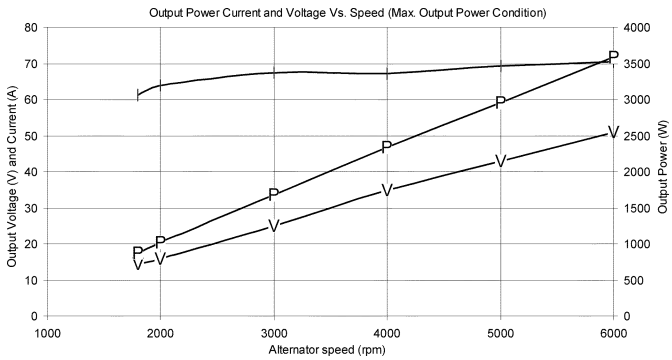

Fig. 17. Output current, voltage, and power of the Lundell alternator versus alternator speed at maximum output-power condition.

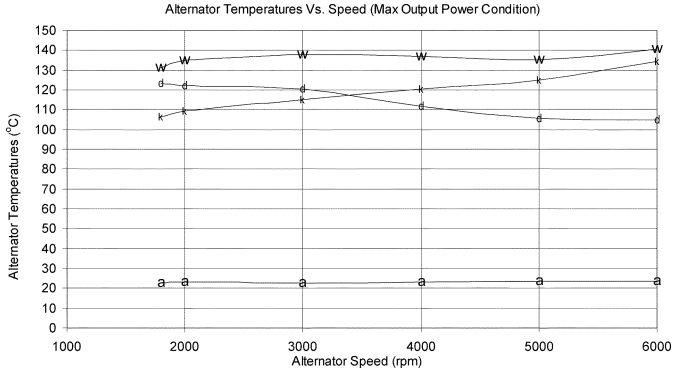

Fig. 18. Measured temperatures of the Lundell alternator versus alternator speed at maximum output-power condition.

as the alternator speed increases. The measured temperature distribution of the Lundell alternator at load-matched conditions versus alternator speed is illustrated in Fig. 18. Because the increase of stator winding conduction loss is relatively small and the cooling effect increases as the alternator speed increases, the temperature increase of the stator winding is relatively small, from 131 °C at 1800 r/min to 140 °C at 6000 r/min. See (11)–(13), shown at the bottom of the next page.

We now apply the proposed thermal model to the load-matched case. The formulas for the six thermal resistances have been expressed in (2) to (7) and their values versus different alternator speeds have been plotted in Fig. 15. The winding conduction loss P_w can be obtained by measuring the line currents and the winding resistance, as described in (14)

$$P_w = I_A^2 R_A + I_B^2 R_B + I_C^2 R_C \tag{14}$$

where R_A, R_B, and R_C are the ac winding resistance of phase *A*, *B*, and *C*, respectively (see Appendix B) and I_A, I_B, and I_C are the root-mean-square (rms) line currents of phase *A*, *B*, and *C*, respectively. It is also possible to predict these using the alternator model of [8], or through simulation.

The power dissipation of the diode rectifier can be obtained by summing the power loss of each individual power diode which is equal to the time average value of the product of the instantaneous diode voltage v_d and diode current i_d in one cycle. By measuring the instantaneous values of v_d and i_d with a digital

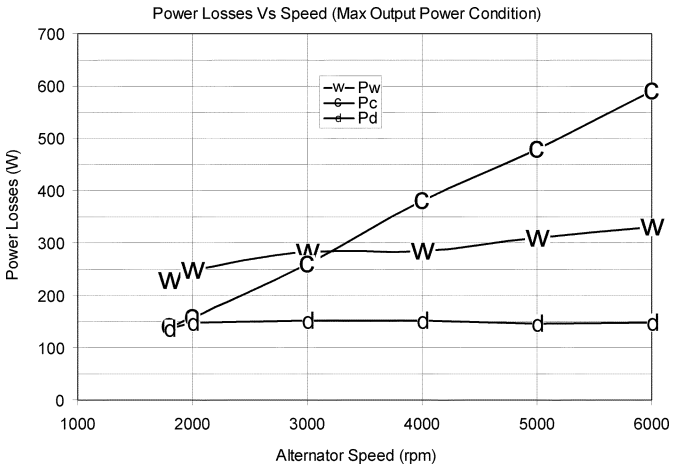

Fig. 19. Measured stator winding conduction loss P_w, diode rectifier loss P_d, and estimated stator core loss P_c of the Lundell alternator at maximum output-power condition.

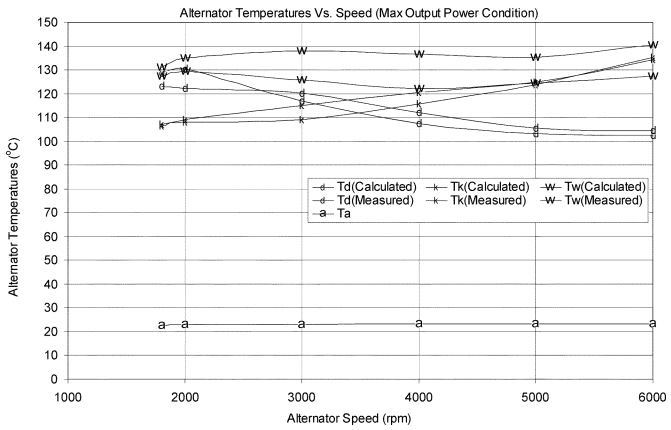

Fig. 20. Measured and calculated diode temperature T_d, case temperature T_k, and stator winding temperature T_w of the Lundell alternator at maximum output-power condition, and measured ambient temperature T_a.

oscilloscope, the power loss of one diode P_{diode} can be calculated as

$$P_{\text{diode}} = \frac{1}{N}\sum_{i=1}^{N} v_d(i) \times i_d(i) \tag{15}$$

where N is the number of samples in one cycle taken by a digital oscilloscope. Again, this could alternatively be predicted using the model [8] or via simulation.

Since there is no direct method to measure the stator core loss of the alternator, the core loss can be obtained by subtracting the stator winding loss from the total stator loss, as described in Appendix C. Alternatively, core loss can be predicted using the Steinmetz equation [12] and knowledge of the alternator construction.

The measured powers of stator winding loss P_w, diode rectifier loss P_d, and approximated stator core loss P_c of the Lundell alternator versus alternator speed at maximum output power condition are plotted in Fig. 19. Substituting the three power losses in Fig. 19 and the six thermal resistance in Fig. 15 into (11)–(13), the diode temperature T_d, the case temperature T_k, and the winding temperature T_w of the Lundell alternator operating at the maximum output-power condition can be calculated and illustrated in Fig. 20. The match between actual and predicted temperatures is found to be quite good. Because the underestimated stator core loss is used, the calculated alternator temperatures are less than the measured temperatures. From Fig. 20, the maximum error of the calculated winding temperature, compared with the measured winding temperature, is about $6-14.6$ °C out of 136.7 °C. For purposes of integrating an SMR circuit into the alternator, the ability to accurately predict the diode plate temperature is of special importance. Note that the model predicts diode temperature quite well, with a maximum error of 8.2%.

VII. Conclusion

Temperature profiles of a typical Lundell alternator with both 14-Vdc load and maximum load-matched output-power conditions have been investigated. Major heat sources of the alternator have been identified. A simple thermal model for Lundell alternators is proposed. Procedures for acquiring the model parameters (i.e., power losses and thermal resistance), have been detailed. Using the thermal model, the temperature profile of a Lundell alternator can be predicted analytically. The thermal model has been validated by comparing the calculated temperature distribution with measurement. It is expected that

$$\Delta T_{da} = \frac{\left\{\begin{array}{c}\left[\left((R_{ka}+R_{dk})R_{dw}+(R_{wk}+R_{dk})R_{ka}+R_{dk}R_{wk}\right)R_{wa}+\left((R_{wk}+R_{dk})R_{ka}+R_{dk}R_{wk}\right)R_{dw}\right]P_d \\ +\left((P_c+P_w)R_{ka}R_{dw}+R_{ka}P_cR_{wk}\right)R_{wa}+R_{ka}P_cR_{dw}R_{wk}\end{array}\right\}R_{da}}{\begin{array}{c}\left[\left(R_{ka}+R_{dk}+R_{da}\right)R_{dw}+\left(R_{ka}+R_{da}+R_{dk}\right)R_{wk}+R_{dk}R_{ka}\right]R_{wa} \\ +R_{dw}\left[\left(R_{da}+R_{dk}\right)R_{ka}+\left(R_{ka}+R_{dk}+R_{da}\right)R_{wk}\right]\end{array}} \tag{11}$$

$$\Delta T_{ka} = \frac{\left\{\begin{array}{c}\left[\left((R_{dk}+R_{wk}+R_{dw})P_d+(R_{wk}+R_{dw})P_c+R_{dw}P_w\right)R_{wa}+P_dR_{dw}R_{wk}+P_cR_{wk}R_{dw}\right]R_{da} \\ +\left((R_{wk}+R_{dw})P_c+R_{dw}P_w\right)R_{dk}R_{wa}+P_cR_{dk}R_{wk}R_{dw}\end{array}\right\}R_{ka}}{\begin{array}{c}\left[\left(R_{ka}+R_{dk}+R_{da}\right)R_{dw}+\left(R_{ka}+R_{da}+R_{dk}\right)R_{wk}+R_{dk}R_{ka}\right]R_{wa} \\ +R_{dw}\left[\left(R_{da}+R_{dk}\right)R_{ka}+\left(R_{ka}+R_{dk}+R_{da}\right)R_{wk}\right]\end{array}} \tag{12}$$

$$\Delta T_{wa} = \frac{\left\{\begin{array}{c}\left[\left((R_{ka}+R_{wk})P_w+(P_d+P_c)R_{ka}\right)R_{da}+\left((R_{wk}+R_{dk})R_{ka}+R_{dk}R_{wk}\right)P_w+P_cR_{dk}R_{ka}\right]R_{dw} \\ +\left[\left(R_{wk}+R_{dk}\right)P_d+R_{wk}P_c\right)R_{ka}+P_dR_{dk}R_{wk}\right]R_{da}\end{array}\right\}R_{wa}}{\begin{array}{c}\left[\left(R_{ka}+R_{dk}+R_{da}\right)R_{dw}+\left(R_{ka}+R_{da}+R_{dk}\right)R_{wk}+R_{dk}R_{ka}\right]R_{wa} \\ +R_{dw}\left[\left(R_{da}+R_{dk}\right)R_{ka}+\left(R_{ka}+R_{dk}+R_{da}\right)R_{wk}\right]\end{array}}. \tag{13}$$

TABLE I
THERMAL AND ELECTRICAL ANALOGY

Thermal Circuit	Electrical Circuit
Thermal Resistance, R_{th}	Resistance, R
Heat Power Flow, Q	Current, I
Temperature Difference, ΔT	Potential (or Voltage) Difference, ΔV
Thermal Conductivity, k	Electrical Conductivity, σ

the presented models and measurement procedures will be of great value in designing alternator with embedded power-electronic controls. From the measured temperature distribution of an alternator, it is envisaged that embedding switching power electronics into the Lundell alternator with low manufacturing cost is possible by thermally isolating the power-electronics assembly from the alternator machine.

APPENDIX A
THERMAL AND ELECTRICAL CIRCUITS ANALOGY AND SOLUTION OF THE THERMAL RESISTANCE

A. Thermal and Electrical Analogy

In a thermal circuit, the path for heat transfer is represented by a thermal resistance, which is analogous to a resistance in the electrical circuit. Heat power flowing through and temperature difference across a thermal resistance is respectively analogous to the current and potential difference across the resistance in the electrical circuit. The thermal and electrical analogy are tabulated in Table I. There are three modes of heat transfer: heat conduction, convection, and radiation. However, in the alternator system, the heat transfer is mainly due to heat conduction and convection, and the effect of radiation can be neglected. The following describes how the paths for conductive and convective heat transfer can be represented by thermal resistance; a more detailed theory of heat transfer can be found in [13].

1) Heat Conduction: When temperature gradient ∇T exists within a body, heat power Q flows from the high-temperature region to the low-temperature region, as described by the Fourier's law of heat conduction

$$q = -k\nabla T \tag{A.1}$$

where k ($\mathrm{Wm^{-1}K^{-1}}$) is the conductivity of the body, and q ($\mathrm{Wm^{-2}}$) is the heat flux (i.e., heat power flows per unit area).

Consider an object with cross-section area A and length l, as shown in Fig. 21, heat power transfers from one end, with temperature T_1 to the other end, with temperature T_2, is related by

$$Q = \frac{k \cdot A}{l}(T_1 - T_2) = \frac{T_1 - T_2}{R_{\mathrm{th(cond)}}} \tag{A.2}$$

where $R_{\mathrm{th(cond)}} = l/k \cdot A$ ($\mathrm{K \cdot W^{-1}}$) represents the thermal resistance by heat conduction.

When the thermal conductivity k is analog to the electrical conductivity σ, (A.2) becomes the Ohm's law analogy describing a current I flowing through the object

$$I = \frac{\sigma \cdot A}{l}(V_1 - V_2) = \frac{V_1 - V_2}{R} \tag{A.3}$$

where V_1 and V_2 are the voltage across the two ends.

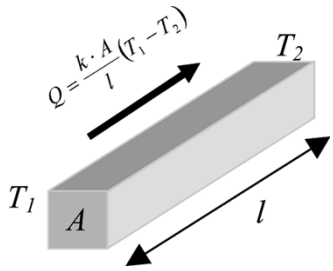

Fig. 21. Heat power transfer in a rod by heat conduction.

2) Heat Convection: Heat transfer by convection occurs when heat energy is carrying away from the surface of a body by a moving fluid. From the Newton's law of cooling, heat power flowing from the surface of a body can be expressed as

$$Q = hA_s\left(T_{\mathrm{surf}} - T_{\mathrm{fluid}}\right) \tag{A.4}$$

where h is the film coefficient or heat transfer coefficient, and A_s is the area of the body surface from which the fluid carries heat away from the body (the "wetted" area).

From (A.4), the path for heat transfer by convection can be represented by a thermal resistance

$$R_{\mathrm{th(conv)}} = \frac{1}{hA_s} = \frac{T_{\mathrm{surf}} - T_{\mathrm{fluid}}}{Q}. \tag{A.5}$$

B. Solution of the Thermal Resistance in the Alternator Model

The six unknown thermal resistance in the thermal model shown in Fig. 9 can be solved by setting up six independent equations. By using nodal analysis in electric-circuit theory, three equations can be set up when the stator windings are the heat source and no current is flowing through the rectifier.

At node T_d

$$\left(\Delta T_{da(w)} - \Delta T_{ka(w)}\right)\frac{1}{R_{dk}} + \Delta T_{da(w)}\frac{1}{R_{da}} = 0. \tag{A.6}$$

At node T_k

$$\left(\Delta T_{ka(w)} - \Delta T_{da(w)}\right)\frac{1}{R_{dk}} + \left(\Delta T_{ka(w)} - \Delta T_{wa(w)}\right)\frac{1}{R_{wk}} + \Delta T_{ka(w)}\frac{1}{R_{ka}} = 0. \tag{A.7}$$

At node T_w

$$\left(\Delta T_{wa(w)} - \Delta T_{ka(w)}\right)\frac{1}{R_{wk}} + \left(\Delta T_{wa(w)} - \Delta T_{da(w)}\right)\frac{1}{R_{dw}} + \Delta T_{wa(w)}\frac{1}{R_{wa}} = P_w. \tag{A.8}$$

Similarly, three more independent equations can be set up when the rectifier becomes the heat source and no current is flowing through the stator windings.

At node T_d

$$\left(\Delta T_{da(d)} - \Delta T_{ka(d)}\right)\frac{1}{R_{dk}} + \Delta T_{da(d)}\frac{1}{R_{da}} = P_d. \tag{A.9}$$

At node T_k

$$\left(\Delta T_{ka(d)} - \Delta T_{da(d)}\right)\frac{1}{R_{dk}} + \left(\Delta T_{ka(d)} - \Delta T_{wa(d)}\right)\frac{1}{R_{wk}} + \Delta T_{ka(d)}\frac{1}{R_{ka}} = 0. \quad \text{(A.10)}$$

At node T_w

$$\left(\Delta T_{wa(d)} - \Delta T_{ka(d)}\right)\frac{1}{R_{wk}} + \left(\Delta T_{wa(d)} - \Delta T_{da(d)}\right)\frac{1}{R_{dw}} + \Delta T_{wa(d)}\frac{1}{R_{wa}} = 0. \quad \text{(A.11)}$$

R_{da} and R_{dk} are solved from (A.6) and (A.9) and shown in (2) and (3), respectively. By substituting R_{dk} in (3) into (A.7) and (A.10), R_{ka} and R_{wk} are solved and shown in (4) and (5), respectively. Similarly, R_{dw} and R_{wa} can be solved by substituting R_{wk} in (5) into (A.8) and (A.11), and are shown in (6) and (7), respectively.

APPENDIX B
ALTERNATOR WINDING RESISTANCE

The measured stator dc winding resistance is 26.58 and 37.96 $\mathrm{m\Omega}$ at 21 °C and 150 °C, respectively. The dc resistance values of the three stator windings are found to be approximately identical. Since the dc resistance of copper wire increases linearly with temperature, the stator dc winding resistance is given as

$$R_{dc}(T) = 0.088\,22T_w + 0.631 \quad \text{(B.1)}$$

where R_{dc} is in mΩ, and T_w is in Kelvin.

When the winding temperature is equal to or higher than room temperature of about 293 K, the term T_w is much larger than the constant term in (B.1). Equation (B.1) can be approximated as (B.2) in order to simplify the following ac resistance calculation:

$$R_{dc}(T) \approx 0.088\,22T_w \quad (T_w > 293\,\mathrm{K}). \quad \text{(B.2)}$$

From [14], the ac-to-dc resistance factor is given by

$$\frac{R_{\mathrm{ac}}}{R_{\mathrm{dc}}} \approx 1 + \frac{\Psi}{3}\Delta^4 \quad \text{(B.3)}$$

where Ψ is a constant depends on the winding geometry, and Δ is the ratio of the wire thickness d to the skin depth δ, i.e., $\Delta = d/\delta$ and $\delta = 1/\sqrt{\pi f \mu \sigma}$.

From (B.3), the ac winding resistance $R_{\mathrm{ac}}(T)$, at temperature T, can be expressed as

$$R_{\mathrm{ac}}(T) \approx R_{\mathrm{dc}}(RT)K_T\left(1 + \frac{\Psi}{3}\Delta^4(T)\right) \quad \text{(B.4)}$$

where K_T is the ratio of R_{dc} at temperature T to that at room temperature RT (i.e., $K_T \equiv R_{\mathrm{dc}}(T)/R_{\mathrm{dc}}(RT)$).

The ratio of the value of Δ at temperature T to that at room temperature RT can be expressed as

$$\frac{\Delta(T)}{\Delta(RT)} = \frac{\delta(RT)}{\delta(T)} = \sqrt{\frac{\sigma(T)}{\sigma(RT)}} = \frac{1}{\sqrt{K_T}}. \quad \text{(B.5)}$$

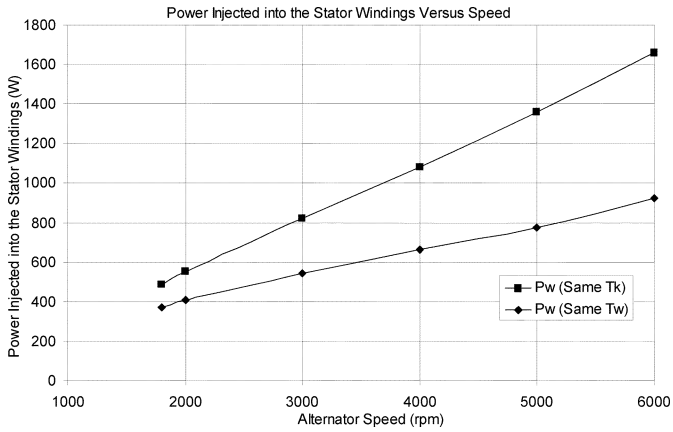

Fig. 22. Powers injected into the stator winding to set either the winding or the case temperature are the same as that when the alternator is operating at maximum output-power condition.

Substituting (B.5) into (B.4), the ac winding resistance as a function of frequency f and temperature T can be derived as

$$\begin{aligned} &R_{\mathrm{ac}}(T) \\ &\approx R_{\mathrm{dc}}(RT)K_T\left(1 + \frac{\Psi}{3}\frac{1}{K_T^2}\Delta^4(RT)\right) \\ &\Rightarrow R_{\mathrm{ac}}(T) \approx R_{\mathrm{dc}}(RT)K_T\left(1 + \frac{\Psi}{3}\frac{1}{K_T^2}\left(\frac{d}{\delta(RT)}\right)^4\right) \\ &\Rightarrow R_{\mathrm{ac}}(T) \approx R_{\mathrm{dc}}(RT)K_T\left(1 + \frac{\Psi}{3}\frac{1}{K_T^2}d^4\left[\pi f \mu \sigma(RT)\right]^2\right). \end{aligned} \quad \text{(B.6)}$$

The windings are made of copper, $\mu = 4\pi \times 10^{-7}\,\mathrm{H/m}$ and $\sigma = 5.8 \times 10^7$ S/m at room temperature. The measured ac winding resistance at 600 Hz is about 32.7 mΩ at room temperature. From (B.2), the dc resistance at room temperature of 21 °C is about 26 mΩ. The diameter of the copper wire is 1.6 mm and the porosity factor for round conductors is $\sqrt{\pi}/2$. Thus, from (B.6), the value of Ψ of the alternator under test can be calculated as

$$\begin{aligned} \Psi &= \frac{3}{d^4\left[\pi f \mu \sigma(RT)\right]^2}\left[\frac{R_{\mathrm{ac}}(RT)}{R_{\mathrm{dc}}(RT)} - 1\right] \\ &= \frac{3}{(1.6 \times 10^{-3} \times \frac{\sqrt{\pi}}{2})^4\left[\pi\,(600)\,(4\pi \times 10^{-7})\,(5.8 \times 10^7)\right]^2} \\ &\quad \times \left[\frac{32.7 \times 10^{-3}}{26 \times 10^{-3}} - 1\right] \\ &\approx 10.13. \end{aligned}$$

APPENDIX C
CORE LOSS ESTIMATION

The total stator loss of an operating alternator is approximated by injecting a dc current to the stator winding as shown in Fig. 11 and keeping either the stator winding or the case temperature as the same as that when the alternator is operating. The total stator loss is approximated by the injected power into the stator winding.

When the alternator is operating, part of the heat source comes from the stator core. However, when power is injected into the stator winding, heat flows from node w to node k and

temperature at node k are lower than that at node w. Thus, when the total power loss of the stator is approximated by the injected stator winding power $P_{w(\text{same Tk})}$ as proposed above, an additional injected power is required to compensate the additional temperature drop across R_{wk} due to the flow of the core loss component through R_{wk} and the total stator loss would be overestimated.

Based on superposition theory, the heat sources P_w and P_c, can be considered separately. When the alternator is operating and only P_c is considered, some part of P_c will flow through R_{wk} from node k to node w and temperature at node w is lower than that at node k. Thus, when the total power loss of the stator is approximated by the injected power $P_{w(\text{same } Tw)}$ so that the winding temperature is the same as that of an operating alternator, the total stator loss would be underestimated. However, because the thermal resistance value of R_{ka} is much smaller than the sum of R_{wk} and R_{wa}, only a small portion of P_c flows through the R_{wk} branch. Besides, the value of R_{wk} is very small, so the temperature drop across R_{wk} is small. As a result, the magnitude of error of $P_{w(\text{same } Tw)}$ for estimating the total stator loss is less than that of $P_{w(\text{same } Tk)}$.

Fig. 22 shows the required powers injected into the stator winding to set either the winding or the case temperature the same as that when the alternator is operating at maximum output-power condition (which is indicated by the straight line in Fig. 16). Since $P_{w(\text{same } Tk)}$ overestimates and $P_{w(\text{same } Tw)}$ underestimates the total stator loss, the actual total stator loss should be between $P_{w(\text{same } Tw)}$ and $P_{w(\text{same } Tk)}$. Since the magnitude of error of $P_{w(\text{same } Tk)}$ for approximating the total stator loss is smaller, the stator core loss is approximated by subtracting the stator winding loss from $P_{w(\text{same } Tk)}$.

REFERENCES

[1] R. Erikson, "ISG integrated starter generator," in *Kurbelwellenstart-generator (KSG) – Basis für Zukünftige Fahrzeugkonzepte*, A. Krappel, Ed. Berlin, Germany: Expert Verlag, 1999, ch. 7, pp. 99–112.

[2] J. M. Miller, "Multiple voltage electrical power distribution system for automotive applications," in *Proc. Intersociety Energy Conversion Conf.*, Washington, DC, Aug. 1996.

[3] J. M. Miller, D. Goel, D. Kaminski, H.-P. Shoener, and T. M. Jahns, "Making the case for a next generation automotive electrical system," in *Proc. IEEE-SAE Int. Conf. Transportation Electronics (Convergence)*, Dearborn, MI, Oct. 1998.

[4] M. H. Rashid, *Power Electronics Handbook*. New York: Academic, 2001, ch. 31.

[5] D. J. Perreault and V. Caliskan, "Automotive Power Generation and Control," MIT Laboratory for Electromagnetic and Electronic Systems, Tech. Rep. TR-00-003, 2000.

[6] ——, "A new design for automotive alternators," in *Proc. Int. Conf. Transportation Electronics (Convergence 2000)*, Oct. 2000, SAE Paper 2000-01-C084, pp. 583–594.

[7] *Automotive Electric/Electronic Systems*, 2nd ed., Robert Bosch GmbH, Stuttgart, Germany, 1995.

[8] V. Caliskan, D. J. Perreault, T. M. Jahns, and J. G. Kassakian, "Analysis of three-phase rectifiers with constant-voltage loads," in *IEEE Power Electronics Specialists Conf.*, vol. 2, June 1999, pp. 715–720.

[9] R. W. Lewis, K. Morgan, H. R. Thomas, and K. N. Seetharamu, *The Finite Element Method in Heat Transfer Analysis*. New York: Wiley, 1996.

[10] C. E. Tindall and S. Brankin, "Loss-at-source thermal modeling in salient pole alternators using 3-dimensional finite difference techniques," *IEEE Trans. Magn.*, vol. 24, no. 1, pp. 278–281, Jan. 1988.

[11] J. Driesen, R. J. M. Belmans, and K. Hameyer, "Methodologies for coupled transient electromagnetic-thermal finite-element modeling of electrical energy transducers," *IEEE Trans. Ind. Appl.*, vol. 38, no. 5, pp. 1244–1250, Sep./Oct. 2002.

[12] J. Li, T. Abdallah, and C. R. Sullivan, "Improved calculation of core loss with nonsinusoidal waveforms," in *IEEE Ind. Appl. Soc. Annu. Meeting*, vol. 4, Sep. 2001, pp. 2203–2210.

[13] J. H. Lienhard IV and J. H. Lienhard V, *A Heat Transfer Textbook*, 3rd ed. Cambridge, MA: Phlogiston, 2002, ch. 1 and 2.

[14] W. G. Hurley, E. Gath, and J. G. Breslin, "Optimizing the AC resistance of multilayer transformer windings with arbitrary current waveforms," *IEEE Trans. Power Electron.*, vol. 15, no. 2, pp. 369–376, Mar. 2000.

Sai Chun Tang (S'97–M'01) was born in Hong Kong in 1972. He received the B.Eng. (Hons.) and the Ph.D. degrees in electronic engineering from the City University of Hong Kong in 1997 and 2000, respectively.

Currently, he is with the Focused Ultrasound Laboratory, Brigham and Women's Hospital, Harvard Medical School, Boston, MA. After he graduated, he was a Research Fellow with the same university. He was a Visiting Academic with the National University of Ireland Galway, in 2001 and then a Postdoc with the Laboratory for Electromagnetic and Electronic Systems at MIT in 2002. for the development of a noninvasive tumor treatment system using an intensive-focused ultrasound beam. His research interests include high-frequency electromagnetism, low-profile power converter design, and analog electronics.

Dr. Tang received the Best Paper Award (for posters) at The 16th European Conference on Solid-State Transducers (Eurosensors XVI) in 2002. He won the championship of the Institution of Electrical Engineers (IEE) Hong Kong Younger Member Section Paper Contest 2000 and received the first prize of IEEE HK Section Student Paper Contest'97. He is a member of Sigma Xi.

Thomas A. Keim, photograph and biography not available at time of publication.

David J. Perreault (M'98–S'91–M'97) received the B.S. degree from Boston University, Boston, MA, in 1989, and the S.M. and Ph.D. degrees from the Massachusetts Institute of Technology (MIT), Cambridge, in 1991 and 1997, respectively.

Currently, he is the Emanuel E. Landsman Associate Professor of Electrical Engineering and Computer Science, Department of Electrical Engineering and Computer Science, MIT. In 1997, he joined the MIT Laboratory for Electromagnetic and Electronic Systems as a Postdoctoral Associate, and became a Research Scientist in the laboratory in 1999. His research interests include design, manufacturing, and control techniques for power-electronic systems and components, and their use in a wide range of applications.

Dr. Perreault is a member of Tau Beta Pi and Sigma Xi. He received the Richard M. Bass Outstanding Young Power Electronics Engineer Award from the IEEE Power Electronics Society and an ONR Young Investigator Award, and has received two IEEE prize paper awards.